

SPINVERT: A program for refinement of paramagnetic diffuse scattering data

Joseph A. M. Paddison^{1,2}, J. Ross Stewart², and Andrew L. Goodwin^{1,*}

¹ Department of Chemistry, Inorganic Chemistry Laboratory, University of Oxford, South Parks Road, Oxford OX1 3QR, U.K.

E-mail: andrew.goodwin@chem.ox.ac.uk

² ISIS Facility, Rutherford Appleton Laboratory, Harwell Science and Innovation Campus, Didcot, Oxfordshire OX11 0QX, U.K.

Abstract. We present a program (SPINVERT; <http://spinvert.chem.ox.ac.uk>) for refinement of magnetic diffuse scattering data for frustrated magnets, spin liquids, spin glasses, and other magnetically disordered materials. The approach uses reverse Monte Carlo refinement to fit a large configuration of spins to experimental powder neutron diffraction data. Despite fitting to spherically-averaged data, this approach allows the recovery of the three-dimensional magnetic diffuse scattering pattern and the spin-pair correlation function. We illustrate the use of the SPINVERT program with two case studies. First we use simulated powder data for the canonical Heisenberg kagome model to discuss the sensitivity of SPINVERT refinement to both pairwise and higher-order spin correlations. The effect of limited experimental data on the results is also considered. Second, we re-analyse published experimental data on the frustrated system $Y_{0.5}Ca_{0.5}BaCo_4O_7$. The results from SPINVERT refinement indicate similarities between $Y_{0.5}Ca_{0.5}BaCo_4O_7$ and its parent compound $YBaCo_4O_7$, which were overlooked in previous analysis using powder data.

Submitted to: *J. Phys.: Condens. Matter*

1. Introduction

The intense current interest in magnetic materials in which the magnetic moments (“spins”) do not form a periodic arrangement has been fuelled by the observation of strongly-correlated states, including the discovery of emergent magnetic charges in spin-ice materials [1, 2], the observation of excitations with fractional quantum number in quantum spin liquids [3], and the presence of chiral order in otherwise-degenerate states [4]. States such as these—lacking long-range magnetic order, but exhibiting distinctive forms of local order—have been termed “cooperative paramagnets” [5]. The “gold standard” experiment for the study of spin correlations is neutron scattering on a large single crystal sample. Such measurements provide a direct measurement of the Fourier transform of the three-dimensional spin correlation function $I(\mathbf{Q})$. In cooperative paramagnets, neutron scattering experiments often reveal highly-structured diffuse features in reciprocal space—such as the well-known “pinch points”

of spin ice—which can be analysed to characterise the spin correlations in real-space [2, 6].

Unfortunately, however, large single-crystal samples are not available for many interesting materials. This is particularly—but far from exclusively—a problem for newly-synthesised compounds. Consequently, neutron scattering measurements must often be performed on powder (polycrystalline) samples. In a powder neutron scattering experiment, the three-dimensional scattering pattern is collapsed onto a single axis, Q . For magnetic materials which show conventional long-range spin order, this may not actually present a significant problem, since the established technique of magnetic Rietveld refinement can (in favourable cases) provide an unambiguous solution of the magnetic structure based on only the powder-averaged positions and intensities of the magnetic Bragg peaks [7]. In this way, symmetry arguments effectively replace the information which is lost as a result of powder averaging. In cooperative paramagnets, by contrast, the lack of long-range spin order means that there are no magnetic Bragg peaks: the powder average of the scattering pattern shows no sharp features, merely a few diffuse “humps”. As a consequence, there has been no obvious analogue of magnetic Rietveld refinement which can determine the three-dimensional spin correlation function from powder *diffuse* scattering data.

In this paper we introduce a new suite of programs, SPINVERT, which allows determination of the three-dimensional spin correlation function by fitting powder diffuse scattering data. Our program employs reverse Monte Carlo refinement [8, 9] to fit a large configuration of spin vectors to experimental powder data. The positions of spins are fixed at their crystallographic sites throughout the refinement, while their orientations are refined in order to fit the data. The RMC algorithm itself is well-established, having previously been used to study states as diverse as spin glasses [9], ordered magnetic structures [10], and flux-line lattices in superconductors [11]. The algorithm is entirely analogous to a direct Monte Carlo simulation, apart from one important difference: the function which is minimised during the refinement is not an energy term defined by a spin Hamiltonian, but rather the sum of squared residuals which quantifies the level of disagreement between the fit and experimental data. Thus, RMC is not a technique for modelling magnetic *interactions* based on a spin Hamiltonian, but rather a technique for refinement of spin *correlations* based on experimental data [12].

It is clear even from this brief overview that the RMC approach is a simple—even naïve—one. However, for cooperative paramagnets, it is also remarkably powerful. In our previous work [13], we investigated the extent to which three-dimensional information could be recovered from powder diffuse scattering data in the following way. First, powder diffuse scattering patterns were simulated for a number of models of frustrated magnetism. These powder “data” were then fitted using the RMC approach. From these refined spin configurations, we calculated the *three-dimensional* scattering pattern $I(\mathbf{Q})$, and compared the patterns obtained from RMC with the exact results. We found that, for each model we considered, almost all the features of the single-crystal scattering patterns were reproduced by fitting the powder patterns. Consequently, the spin configurations obtained by RMC correctly reproduce the three-dimensional spin correlations of the starting model: they represent one of the degenerate “solutions” of the paramagnetic structure.

Why is the RMC approach so successful? To answer this question, we compare it to alternative “model-independent” approaches. Most such approaches essentially involve fitting a simple form for the radial spin correlation function to the powder

data. In these methods, the connectivity of the crystal structure is not considered; instead, either the magnitude of the spin correlations is fitted for a one-dimensional list of atomic separations (see, *e.g.*, [14, 15]), or the diffuse features are fitted to a broad peak-shape function to estimate the spin correlation length (see, *e.g.*, [16]). However, the crystal structure plays no less significant a role in paramagnets than in ordered magnets: indeed, in a paramagnet the crystal structure completely determines the symmetry and periodicity of the diffuse scattering pattern [17]. Consequently, knowledge of the crystal structure imposes very significant constraints on the form of both the single-crystal and powder scattering. Unlike other model-independent approaches—but in common with approaches using a spin Hamiltonian—RMC refinement uses knowledge of the crystal structure to constrain the spin correlations.

Our paper is organised as follows. First, we introduce our implementation of RMC in detail, and summarise the key equations underpinning the SPINVERT program. Next, we discuss possible ways in which the resulting spin configurations may be analysed, drawing connections with previous work using RMC and other techniques. Finally, we present two case studies intended to illustrate the use of the SPINVERT program. In the first case study, we fit simulated data for the Heisenberg model on the kagome lattice [18, 19], and investigate the effects of limited Q -range and statistical errors on the results which are obtained. In our second case study, we present a new analysis of existing experimental powder data on $\text{Y}_{0.5}\text{Ca}_{0.5}\text{BaCo}_4\text{O}_7$ (from Ref. [15]) in order to clarify the nature of the paramagnetic spin correlations in this material. The results we obtain from SPINVERT analysis indicate some close similarities between $\text{Y}_{0.5}\text{Ca}_{0.5}\text{BaCo}_4\text{O}_7$ and its parent compound YBaCo_4O_7 , that may have been overlooked in previous analyses [15]. We conclude with a discussion of the general advantages and disadvantages of the RMC approach, and some perspectives for future work.

2. Theoretical background

Reverse Monte Carlo method

The general RMC method has been described in detail elsewhere [13, 20]; here we summarise our specific implementation of magnetic RMC. First, a supercell of the crystallographic unit cell is generated. The supercell usually contains several thousand atoms, and periodic boundary conditions are used to avoid edge effects. A classical spin vector with random orientation is assigned to each atom, and the goodness-of-fit to experimental data is calculated:

$$\chi^2 = W \sum_Q \left[\frac{I_{\text{calc}}(Q) - I_{\text{expt}}(Q)}{\sigma(Q)} \right]^2. \quad (1)$$

Here, $I(Q)$ is the powder-averaged magnetic scattering intensity [21], superscript calc and expt denotes calculated and experimental values, $\sigma(Q)$ is an experimental uncertainty, and W is an empirical weighting factor. A spin is then chosen at random from the supercell and rotated by a small amount. This is done by choosing a unit vector \mathbf{s} with random orientation and forming the new spin vector

$$\mathbf{S}_i^{\text{new}} = \frac{\mathbf{S}_i + \Delta \mathbf{s}}{|\mathbf{S}_i + \Delta \mathbf{s}|}, \quad (2)$$

where $0 < \Delta \leq 1$ is the maximum spin move length. In practice, we have found that the final results obtained in RMC fitting are almost independent of the value of Δ ; a

value $\Delta = 0.2$ is used by default. After a move is proposed, the change in goodness-of-fit is calculated, and the proposed move is either accepted or rejected according to the Metropolis criteria [22]. This process is repeated until no further reduction in χ^2 is observed. In this way, spins are iteratively rotated to form a configuration for which spin correlations are consistent with experimental data.

Throughout this work, we treat spins as having unit length, with the magnitude of the spin (*i.e.*, the length of the effective magnetic moment) absorbed into an overall intensity scale factor. When fitting experimental data, it is almost always necessary to allow the value of this scale factor s to refine in order to fit the data. The best-fit value of s can be calculated after each proposed move by minimising χ^2 with respect to s , which yields [23]

$$s = \frac{\sum_Q [I_{\text{calc}}(Q)I_{\text{expt}}(Q)] / [\sigma(Q)]^2}{\sum_Q [I_{\text{calc}}(Q)]^2 / [\sigma(Q)]^2}. \quad (3)$$

If the data are placed on an absolute scale, the effective magnetic moment is then determined by the relation

$$\begin{aligned} \mu^2 &= g^2 S(S+1) \\ &= s, \end{aligned} \quad (4)$$

where g is the g-factor. It is possible also to refine a flat or linear-in- Q background in addition to the scale factor; the relevant equations are given in Ref. [23].

Magnetic neutron scattering intensity

The magnetic scattering cross-section is variously denoted $I(\mathbf{Q})$, $S(\mathbf{Q})$ or $d\sigma/d\Omega$. Within the quasistatic approximation and for a single type of spin, it is given as [24]:

$$I(\mathbf{Q}) = C [\mu f(Q)]^2 \frac{1}{N} \left| \sum_{i=1}^N \mathbf{S}_i^\perp \exp(i\mathbf{Q} \cdot \mathbf{r}_i) \right|^2. \quad (5)$$

Here, $f(Q)$ is the magnetic form factor, \mathbf{Q} is the scattering vector (wavevector transfer) and \mathbf{r}_i the position of spin \mathbf{S}_i . The lack of divergence of the magnetic field means that the neutrons only “see” the component of the spin perpendicular to the scattering vector,

$$\mathbf{S}_i^\perp = \mathbf{S}_i - [(\mathbf{Q} \cdot \mathbf{S}_i)\mathbf{Q}] / Q^2. \quad (6)$$

The proportionality constant C is given by

$$C = \left(\frac{\gamma_n r_e}{2} \right)^2 \quad (7)$$

$$= 0.07265 \text{ barn}, \quad (8)$$

where γ_n is neutron magnetic moment in nuclear magnetons and r_e is the classical electron radius. Multiplying out the squared modulus in Eq. (5) allows us to write the scattering cross-section in terms of correlations between pairs of spins,

$$I(\mathbf{Q}) = C [\mu f(Q)]^2 \left[\frac{2}{3} + \frac{1}{N} \sum_{i,j} \mathbf{S}_i^\perp \cdot \mathbf{S}_j^\perp \cos(\mathbf{Q} \cdot \mathbf{r}_{ij}) \right], \quad (9)$$

where $\mathbf{r}_{ij} = \mathbf{r}_j - \mathbf{r}_i$. Here, the double sum over spin pairs excludes the self-correlation terms, for which $i = j$. These terms give an incoherent contribution to the scattering,

which is the additive factor of $\frac{2}{3}$ in (9). In an ideal paramagnet, with zero correlation between different spins, this incoherent scattering is all that is measured. In a real paramagnet, however, some degree of spin correlation is still present, often to temperatures far above the temperature of magnetic ordering.

In order to calculate the powder scattering cross section, we need an expression for the spherical average of (9). An exact expression was given in the 1960s by Blech and Averbach [21], but appears to have been used only rarely since then. Instead, an approximate form—applicable only to an isotropic paramagnet—has often been employed. In this particular case we have

$$\langle \mathbf{S}_i^\perp \cdot \mathbf{S}_j^\perp \rangle = \frac{2}{3} \langle \mathbf{S}_i \cdot \mathbf{S}_j \rangle, \quad (10)$$

so the spin direction is decoupled from \mathbf{Q} . The spherical average over θ is easily performed by writing

$$\mathbf{Q} \cdot \mathbf{r}_{ij} = Q r_{ij} \cos \theta. \quad (11)$$

The result is just a sine Fourier transform of the spin correlations, analogous to the Debye formula or a liquid or a glass [25]:

$$I_{\text{isotropic}}(Q) = \frac{2}{3} C [\mu f(Q)]^2 \left(1 + \frac{1}{N} \sum_{i,j} \mathbf{S}_i \cdot \mathbf{S}_j \frac{\sin Q r_{ij}}{Q r_{ij}} \right). \quad (12)$$

It is important to recognise that this expression is exact only for an isotropic paramagnet in the limit of a large number of spins. It cannot be used to study materials with magnetic anisotropy (*e.g.*, Ising spins). Since (12) is not exact for a general spin configuration, in SPINVERT we use the exact expression of Ref. [21]. We sketch their derivation here. Taking (9) as the starting point, we define a local coordinate system for each pair of spins, i, j . The local \mathbf{z} axis is directed along the vector separating the pair of spins; the local \mathbf{x} axis is perpendicular to \mathbf{z} and lies the plane of \mathbf{S}_i ; and \mathbf{y} is the remaining vector in a right-handed set. This gives for the coordinate axes: $\mathbf{z} = \mathbf{r}_{ij}/r_{ij}$, $\mathbf{x} = [\mathbf{S}_i - (\mathbf{S}_i \cdot \mathbf{z}) \mathbf{z}] / |\mathbf{S}_i - (\mathbf{S}_i \cdot \mathbf{z}) \mathbf{z}|$, and $\mathbf{y} = \mathbf{z} \times \mathbf{x}$. With this local coordinate system, we apply the identity

$$\mathbf{S}_i^\perp \cdot \mathbf{S}_j^\perp = \sum_{\alpha, \beta} \left(\delta^{\alpha\beta} - \frac{Q^\alpha Q^\beta}{Q^2} \right) S_i^\alpha S_j^\beta \quad (13)$$

where, from Fig. 1, the components $\alpha, \beta \in [x, y, z]$ of \mathbf{Q} are given in spherical coordinates by

$$\mathbf{Q} = [Q \sin \theta \cos \varphi, Q \sin \theta \sin \varphi, Q \cos \theta]. \quad (14)$$

Substituting (14) into (13), and the result into (9), gives an expression for $I(\mathbf{Q}) = I(Q, \theta, \varphi)$. The integrals over θ and φ can then be done by hand, which gives the final result

$$I(Q) = C [\mu f(Q)]^2 \left\{ \frac{2}{3} + \frac{1}{N} \sum_{i,j} \left[A_{ij} \frac{\sin Q r_{ij}}{Q r_{ij}} + B_{ij} \left(\frac{\sin Q r_{ij}}{(Q r_{ij})^3} - \frac{\cos Q r_{ij}}{(Q r_{ij})^2} \right) \right] \right\}. \quad (15)$$

in which

$$A_{ij} = S_i^x S_j^x, \quad (16)$$

$$B_{ij} = 2S_i^z S_j^z - S_i^x S_j^x. \quad (17)$$

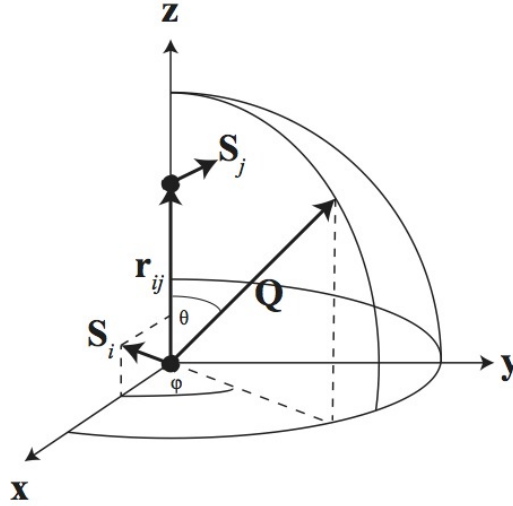


Figure 1. Local spherical coordinate system used for calculation of the powder-averaged neutron scattering intensity.

The sum is taken over all pairs of spins which are separated by radial distances $0 < r_{ij} \leq r_{\max}$; when periodic boundary conditions are imposed, the maximum radial distance r_{\max} is given by half the length of the shortest side of the RMC supercell (“box”).

We end this section by anticipating a common criticism of the RMC approach. It is sometimes argued that the use of a large supercell means that the number of parameters p to be estimated greatly exceeds the number of data points d . The number of parameters is often counted as $p = 2N$ for N spins (since each spin has two rotational degrees of freedom), which indeed is usually greater than n . It is implicit here that the number of degrees of freedom of the RMC fit is calculated using the standard expression $\nu = n - p$. However, this is only applicable when the function which is fitted to the data is linear in the parameters. Since the magnetic scattering cross-section depends on the dot product of pairs of spins, this is not the case, and the effective number of parameters is not well-defined. Moreover, the quantity of interest from Monte Carlo simulations—both direct and reverse—is also not the orientations of individual spins, but rather the correlations between spin-pairs. Consequently, the effectiveness of RMC is not well assessed by such arguments, and is better judged by its performance in real-world applications.

3. Performing SPINVERT refinements: some guidelines

In order to perform a refinement using SPINVERT only a few essential pieces of information are required. First, we need four pieces of experimental information about the system being studied:

- (i) *Experimental powder diffuse scattering data.* The input data should contain only *magnetic* diffuse scattering. Ideally the data will have been obtained using neutron polarisation analysis to isolate the magnetic signal [26]. However, data for which the magnetic signal has been obtained by subtraction of a very high-temperature

dataset from a lower-temperature dataset can also be used. We emphasise that the quality of the results ultimately obtained is entirely dictated by the quality of the data; some guidelines in this respect are given in Section 5.

- (ii) *Crystallographic details: lattice parameters and fractional coordinates of atoms in the crystallographic unit cell.* The SPINVERT program requires that the specified unit cell has orthogonal axes. For hexagonal or rhombohedral systems it is necessary to define a larger orthogonal unit cell for use in SPINVERT. It is further assumed that all atoms in the unit cell have identical magnetic properties (magnetic moments and magnetic form factors), though all atoms need not be crystallographically equivalent. The atom positions are not all required to be occupied by a spin, so it is possible to refine data for systems with substitutional (but not positional) disorder.
- (iii) *Magnetic form factor.* An accurate parameterisation of the magnetic form factor is likely to prove important in SPINVERT refinement, probably to a greater extent than in conventional Rietveld refinement [27]. If the magnetic form factor is not well approximated by tabulated functions, it may be worth performing an accurate measurement to determine it before proceeding.
- (iv) *Single-ion anisotropy.* Spin anisotropy may be fixed by giving the direction of the easy axis for each atom in the unit cell (for Ising spins), or the direction perpendicular to the easy plane (for XY spins). Even if Heisenberg spins are specified, it is still possible for the refinement to produce anisotropic spin configurations, should this be required to fit the data. However, there are almost certainly many more ways of fitting the data in which spins do *not* point along their anisotropy axes, so SPINVERT is likely to underestimate the extent of magnetic anisotropy [13]. Therefore, if other measurements indicate that spins behave as essentially pure Ising or XY variables, we suggest constraining the spin anisotropy accordingly.

There are also four main options concerning the SPINVERT refinement itself:

- (i) *Weight.* The weight, W in (1), is equivalent to inverse temperature in a direct MC simulation, and determines the proportion of “bad” moves that are accepted despite leading to an increase in χ^2 —that is, how closely the data as a whole are fitted. Its value can be freely specified by the user. In practice, the value of W should be chosen such that the fit reproduces the real features of the data without over-fitting to the experimental errors. A good starting point is often to choose W such that between 25% and 75% of the “bad” moves are accepted when the refinement has converged.
- (ii) *Box size.* The size of the spin configuration, given by the number of unit cells along each Cartesian direction which make up the RMC supercell. The maximum correlation length which can be modelled is given by one half the length of the shortest side of the box, so a larger box is needed to reproduce sharper features in $I(Q)$. However, once a sufficiently large box has been identified, there is nothing to be gained by increasing the box size further—doing so merely gives the refinement additional degrees of freedom to vary the long-range spin correlations, which it may do by fitting to high-frequency components (*e.g.*, noise) in the experimental data.
- (iii) *Maximum simulation time.* In general, refinements should be run until no reduction is seen in χ^2 . The number of moves required depends on the data,

the system and the refinement parameters. In practice, $\sim 10^3$ moves per spin is often sufficient.

- (iv) *Intensity scale and background corrections.* When refining experimental data it is almost always necessary to treat the overall intensity scale as a fitting parameter. This is the case when the data have not been placed on an absolute intensity scale, and/or the magnitude of the magnetic moment is not known precisely. In some cases, the minimum in χ^2 can be quite flat as a function of the scale. Then the uncertainty in the scale may be the main source of error in quantities derived from the refinement (*e.g.*, spin correlation length). The uncertainty in derived quantities may be determined, for an assumed uncertainty in the scale, by performing separate refinements with the scale factor fixed at (say) $\pm 5\%$ of its refined value. It is also possible to refine a flat or linear-in- Q background term; however, this should not be done unless necessary, since it introduces an extra parameter into the fit.

The key output from SPINVERT is a spin configuration—a file containing a list of spin vectors, with their corresponding positions in the RMC supercell. An individual spin configuration represents a snapshot picture of a possible arrangement of spins which is consistent with experimental data. In this sense, a spin configuration represents a magnetic structure “solution”. A direct consequence of the absence of long-range magnetic order is that this magnetic structure solution cannot be unique: running the reverse Monte Carlo program again will produce a different spin configuration, which may be thought of as a second snapshot taken a long time after the first. In fact, it is generally important to run RMC simulations several times and average calculated quantities, so that a degree of statistical confidence can be obtained in the results. In the following section, we consider how the spin configurations obtained from RMC can be mined for information about the system properties.

4. Analysis of paramagnetic spin configurations

Once RMC refinements have been performed, the next—and most interesting—stage of the analysis can proceed: unravelling the actual physics which is contained in the spin configurations. Since paramagnetic spin configurations are not unique or periodic, there is no way to describe them that is at once comprehensive and general while using few parameters. This point is equally applicable to disordered spin configurations obtained from other techniques (such as direct Monte Carlo simulation), and reflects a general problem of how to characterise disordered states [28, 29]. To obtain the fullest understanding possible, it is often useful to calculate quantities in both real and reciprocal space: the real-space picture identifies the local spin correlations, whereas the reciprocal-space picture identifies periodicities and long-range components to the correlations [30]. To facilitate this kind of analysis, the associated program SPINCORREL plots real-space spin correlation functions, and the program SPINDIFF calculates the three-dimensional magnetic scattering pattern $I(\mathbf{Q})$.

Real-space: spin correlation functions

It is tempting to try examining directly the orientations of spins within the configuration, but the lack of periodicity means that meaningful patterns are often

hard to discern. Instead, it is better to plot spin-pair correlation functions, which provide a measure of how some property of spin-pairs varies as a function of the separation of the pair of spins. In general,

$$\langle f(\mathbf{S}(\mathbf{0}), \mathbf{S}(\mathbf{r})) \rangle = \frac{1}{N} \sum_i^N f(\mathbf{S}_i, \mathbf{S}_j), \quad (18)$$

where $f(\mathbf{S}_i, \mathbf{S}_j)$ is some function of a central spin \mathbf{S}_i and a spin \mathbf{S}_j at vector \mathbf{r} away from it, and an average is performed over all spins in the configuration as centres. The powder diffraction pattern is essentially a direct measurement of the Fourier transform of the radial spin correlation function $\langle \mathbf{S}(0) \cdot \mathbf{S}(r) \rangle = \langle \cos \varphi \rangle$, which measures the average scalar product of pairs of spins separated by distance r . For a spin configuration, this average is performed by taking each spin \mathbf{S}_i in turn, and then averaging the spin correlations over its Z_{ij} neighbours, \mathbf{S}_j , which coordinate it at distance r :

$$\langle \mathbf{S}(0) \cdot \mathbf{S}(r) \rangle = \frac{1}{n(r)} \sum_i^N \sum_j^{Z_{ij}(r)} \mathbf{S}_i \cdot \mathbf{S}_j, \quad (19)$$

where $n(r)$ is given by

$$n(r) = \sum_i^N Z_{ij}(r), \quad (20)$$

with $Z_{ij}(r)$ the number of spins j which coordinate a central spin i at distance r .

There are many other correlation functions which have been invented to demonstrate various aspects of structures; some examples are considered in the case studies which follow. In structures involving triangular motifs it may be useful to plot the correlation function of the vector or scalar chirality, defined in Ref. [19], or the spin nematic correlation function [Section 5]. In polarised neutron scattering experiments on single-crystal samples it is possible to separate the different Cartesian components of the scattering function with different crystal orientations [2]; the spin-flip and non-spin-flip scattering cross-sections which are measured are also accessible from SPINVERT refinements. In Section 5 we will consider the *three-dimensional* spin correlation function, the real-space analogue of the three-dimensional scattering function $I(\mathbf{Q})$. Finally, we note that SPINVERT refinements provide access not only to the configurational average of correlation functions, but also to their distributions. For example, $\langle \cos \psi \rangle = -0.5$ may well indicate 120° correlations, but could also result from a bimodal distribution of correlations centred at 90° and 180° .

Reciprocal space: magnetic scattering functions

The three-dimensional magnetic scattering pattern $I(\mathbf{Q})$ can reveal important properties of frustrated magnets that are not always so clear in real-space—for example, the power-law correlations in many frustrated magnets appear as “pinch-points” in $I(\mathbf{Q})$. In principle, calculating $I(\mathbf{Q})$ from a spin configuration is straightforward using (5) or (9). While both these equations are mathematically equivalent, it is much faster to compute $I(\mathbf{Q})$ using (5) (which requires $\mathcal{O}(N)$ operations) rather than (9) (which requires $\mathcal{O}(N^2)$ operations). However, choosing to calculate (5) leads to some complications in practice. First, it is not possible to allow for periodic boundary conditions. This is obviously problematic for refinements

which were performed with periodic boundary conditions applied. Second, when the size of the RMC box is large compared to the spin correlation length of the system, the calculated scattering pattern appears very noisy. This seems counterintuitive—since using a larger supercell will reduce the error in $\langle \mathbf{S}(\mathbf{0}) \cdot \mathbf{S}(\mathbf{r}) \rangle$ —but the problem is that as the supercell size is increased, so too does the number of inter-atomic vectors which exceed the spin correlation length. The Fourier transform of these long-wavelength components appears as high-frequency noise in the calculated scattering pattern. In a real experiment, by contrast, this effect is averaged out by the instrumental \mathbf{Q} -resolution [31].

In fact, both these observations suggest the same thing: that it is necessary to restrict the maximum range of the interatomic vectors considered in (5). When periodic boundary conditions are applied, the maximum interatomic vector should not exceed half the box size in each direction. A smaller cutoff may be chosen to correspond to the length-scale at which spin correlations become negligible. The question of how to impose such a cutoff was originally addressed in [31], where it was pointed out that the noise in calculated scattering patterns could be reduced by dividing the RMC supercell into a set of smaller regions called “sub-boxes” or “lots”, and averaging the scattering intensity over all sub-boxes. In effect, this procedure applies a box filter in real space. The calculation proceeds by calculating the three equations in sequence:

$$\mathbf{A}_{\mathbf{R}}(\mathbf{Q}) = \sum_{a=1}^{N_a} \mathbf{S}_{\mathbf{R},a}^{\perp} \exp(i\mathbf{Q} \cdot \mathbf{r}_a), \quad (21)$$

where \mathbf{r}_a is the position of spin $\mathbf{S}_{a,\mathbf{R}}$ within a crystallographic unit cell, \mathbf{R} is a lattice vector giving the origin of the sub-box within the RMC supercell, and the sum runs over the N_a atoms in the unit cell;

$$\mathbf{M}_{\mathbf{R}}(\mathbf{Q}) = \sum_{\mathbf{R}'=\mathbf{R}}^{\mathbf{R}+\mathbf{L}} \mathbf{A}_{\mathbf{R}'}(\mathbf{Q}) \exp(i\mathbf{Q} \cdot \mathbf{R}'), \quad (22)$$

where \mathbf{L} is the sub-box size; and finally a sum over all sub-boxes:

$$I(\mathbf{Q}) = \sum_{\mathbf{R}} |\mathbf{M}_{\mathbf{R}}(\mathbf{Q})|^2. \quad (23)$$

Here, we have used the lattice periodicity to write $\mathbf{r}_i = \mathbf{r}_a + \mathbf{R}$.

The method of sub-boxes greatly reduces the level of noise, and produces calculated scattering patterns in good agreement with experimental data. However, the original method of [31] also has some disadvantages. In particular, the origin of each sub-box was chosen to be a random lattice vector of the supercell with position \mathbf{R} , so a quantitatively different answer is obtained each time the calculation is performed. This problem can be avoided by using every lattice vector \mathbf{R} in the supercell as the origin of a sub-box. However, a straightforward implementation of such an algorithm is very slow. In SPINDIFF, we accelerate the calculation using a fast blurring algorithm often employed in gaming and computer graphics. This takes advantage of the fact that adjacent lots contain the same set of spins, apart from at the lot edges, so that in one dimension we can write

$$\mathbf{M}_{x+1}(\mathbf{Q}) = \mathbf{M}_x(\mathbf{Q}) + \mathbf{A}_{x+L+1} - \mathbf{A}_x. \quad (24)$$

The key point is that applying (24) along each of the Cartesian directions in sequence generates (22) without redundant calculations.

While the method of sub-boxes can improve the appearance of the calculated $I(\mathbf{Q})$, it remains important to have sufficient statistical averaging. Calculated patterns usually appear noisy if they are obtained using only a few thousand spins; to obtain good statistics, it is usually necessary to include $\sim 10^5$ spins in the calculation. The easiest way of achieving this is to average the $I(\mathbf{Q})$ over many individual spin configurations.

As was the case during the SPINVERT refinement, we make some assumptions when calculating $I(\mathbf{Q})$:

- The program calculates only the magnetic scattering; it does not calculate any nuclear scattering.
- The positions of the spins are fixed at their crystallographic positions.
- There is no magnetoelastic coupling.
- All the spins have identical magnetic properties (magnetic form factors and magnetic moments).

Provided these assumptions are satisfied, the program SPINDIFF can be used to calculate the magnetic diffuse scattering for any spin configuration, including those obtained from direct Monte Carlo simulations, spin density-functional theory, and other computational approaches.

5. Kagome Heisenberg magnet

As a first case study we consider the Heisenberg nearest-neighbour antiferromagnet on the kagome lattice. This canonical frustrated model system was studied in detail in the early 1990s, and does not show long-range magnetic order at finite temperature. At low temperature, spins on each triangle form a coplanar 120° arrangement, and there is a macroscopic degeneracy of ways in which these coplanar units can be arranged [32, 18]. Several real materials seem to realise aspects of this behaviour with either classical or quantum spins—for example, hydronium jarosite [33, 34] and herbertsmithite [3, 35]—although in practice there is usually some subtle feature which breaks the degeneracy of ground states.

In order to demonstrate the capabilities of SPINVERT, we first simulate powder diffuse scattering “data” for this model. We consider the classical spin Hamiltonian with nearest-neighbour interactions,

$$H = -\frac{1}{2}J \sum_{\langle i,j \rangle} \mathbf{S}_i \cdot \mathbf{S}_j, \quad (25)$$

at a low temperature $T/J = 0.01$. Direct Monte Carlo simulations for this Hamiltonian were performed for spin configurations of size 3600 spins (comprising ten stacked kagome slabs each of size 360 spins) using periodic boundary conditions. The simulation time was 10^5 proposed MC moves per spin, and 16 independent simulations were performed in order to obtain good statistics for the scattering calculations. The powder diffuse scattering pattern was then calculated from the MC spin configurations using (15), with an arbitrary magnetic form factor (Ho^{3+}) applied. In order to facilitate comparison between powder and single-crystal diffuse scattering patterns, we plot powder scattering patterns as a function of the dimensionless parameter $Q' = aQ/2\pi$, and label high-symmetry points (hkl) in the single-crystal patterns. Powder data were simulated in the range $0 < Q' \leq 5$, and binned at an interval $\Delta Q' = 0.02$.

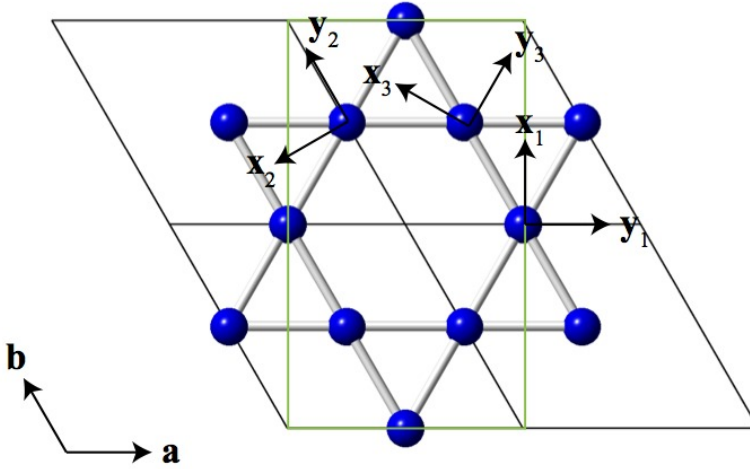


Figure 2. Kagome lattice. The hexagonal unit cell is shown in black, the orthorhombic cell used for RMC refinements in green, and local basis vectors \mathbf{x} used to determine are shown as red arrows. The local \mathbf{x} axis for a given atom points towards the centre of one of the triangles to which the atom belongs, and the local \mathbf{y} axis is a perpendicular vector. Note that due to the point symmetry \mathbf{x} and $-\mathbf{x}$ are equivalent directions, as are \mathbf{y} and $-\mathbf{y}$.

Having obtained these simulated “data” we use them as input data for SPINVERT refinements. Since SPINVERT works with orthogonal axes, it is necessary to convert the hexagonal unit cell with dimensions to an orthorhombic cell containing twice as many atoms; the transformation matrix for this (frequently-encountered) case is given by

$$\begin{bmatrix} \mathbf{a}' \\ \mathbf{b}' \\ \mathbf{c}' \end{bmatrix} = \begin{bmatrix} 1 & 0 & 0 \\ 1 & 2 & 0 \\ 0 & 0 & 1 \end{bmatrix} \begin{bmatrix} \mathbf{a} \\ \mathbf{b} \\ \mathbf{c} \end{bmatrix}.$$

During the following refinements we set the overall intensity scale factor as a parameter to be fitted. Although the absolute scale is already known for the simulated data considered here, this is very unlikely to be the case with experimental data, so we follow the general procedure of allowing a scale factor to refine. We performed SPINVERT refinements for 300 moves per spin, after which time no significant improvement was observed in the value of χ^2 . The fit-to-data obtained using RMC is shown in Fig. 3(a), showing essentially perfect agreement with the data. In fact, this is usually the case for RMC refinements; indeed, if a refinement fails to fit a significant feature in a high-quality dataset, this is usually an indication that something is wrong with the starting model or the refinement parameters.

Having obtained spin configurations in agreement with experiment, we consider how well these fitted spin configurations reproduce the known features of the kagome Heisenberg model. Looking first at reciprocal space, we calculate the single-crystal scattering pattern $I(\mathbf{Q})$ from the SPINVERT refinement and compare it with the corresponding exact pattern obtained from the direct MC simulations [Fig. 3(b)]. Both patterns were calculated using SPINDIFF. Excellent agreement is obtained

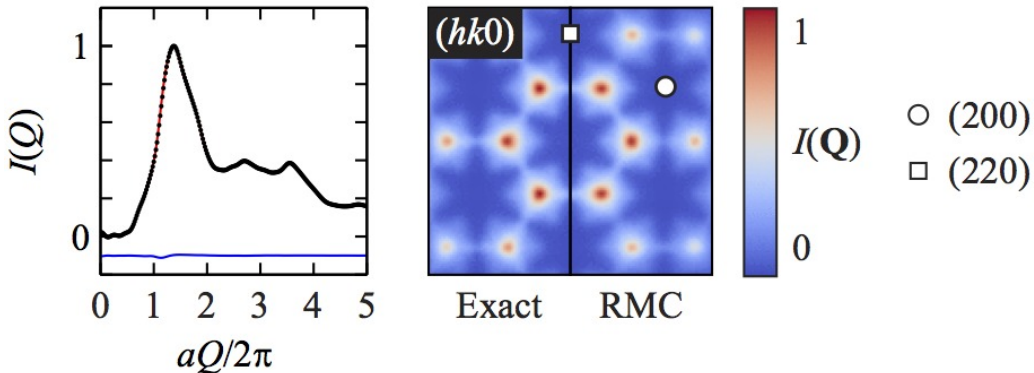


Figure 3. Left: SPINVERT fit to powder data for the antiferromagnetic Heisenberg model on the kagome lattice. Input data are shown as black circles, fit as a red line, and difference (data–fit) as a blue line. Right: Single-crystal scattering in the $(hk0)$ reciprocal-space plane. The panel labelled “Exact” is calculated from the model used to generate the input data (left image); the panel labelled “RMC” is calculated from the SPINVERT refinement of these simulated powder data, as discussed in the text. Both panels are on the same intensity scale.

between the exact result and the SPINVERT prediction, with only a slight blurring of the pattern—corresponding to disordering of the spins—notable in the SPINVERT pattern. We note that this ability to recover the three-dimensional scattering pattern from spherically-averaged data is not limited to this particular model system. In our previous work [13], we considered seven separate systems with different crystal structures and magnetic interactions, and found that the three-dimensional scattering pattern was recoverable from powder data in each case.

We now ask how the spin structures obtained by SPINVERT can be characterised in real space. In Fig. 4(a) we plot the radial spin correlation function $\langle \mathbf{S}(0) \cdot \mathbf{S}(r) \rangle$ for the SPINVERT refinements, and compare it with the exact result. The SPINVERT correlation function is nearly identical to the exact result, typically underestimating the magnitude of the correlations by a few percent. Thus it appears that powder data are very effective at determining the radial spin correlations. While this result is perhaps unsurprising, it is not necessarily the case, since $I(Q)$ and $\langle \mathbf{S}(0) \cdot \mathbf{S}(r) \rangle$ only contain equivalent information in the limit of large Q_{\max} .

Following on from this, a natural question is whether the RMC refinements might afford some sensitivity to higher-order spin correlations. Such correlations are indeed present in the kagome Heisenberg AFM model. At low temperatures ($T/J \lesssim 0.02$), short-range spin *nematic* order develops, so that adjacent triangles of spins tend to lie in a common plane; the mechanism may involve “order by disorder” [18, 19]. The “standard” spin correlation function is insensitive to nematic order, so, following Ref. [18], we define a nematic correlation function which is equal to 1 for a coplanar state:

$$g_n(r) = \frac{3}{2} \left\langle (\mathbf{n}(0) \cdot \mathbf{n}(r))^2 \right\rangle - \frac{1}{2}, \quad (26)$$

where

$$\mathbf{n} = \frac{2}{3\sqrt{3}} (\mathbf{S}_1 \times \mathbf{S}_2 + \mathbf{S}_2 \times \mathbf{S}_3 + \mathbf{S}_3 \times \mathbf{S}_1) \quad (27)$$

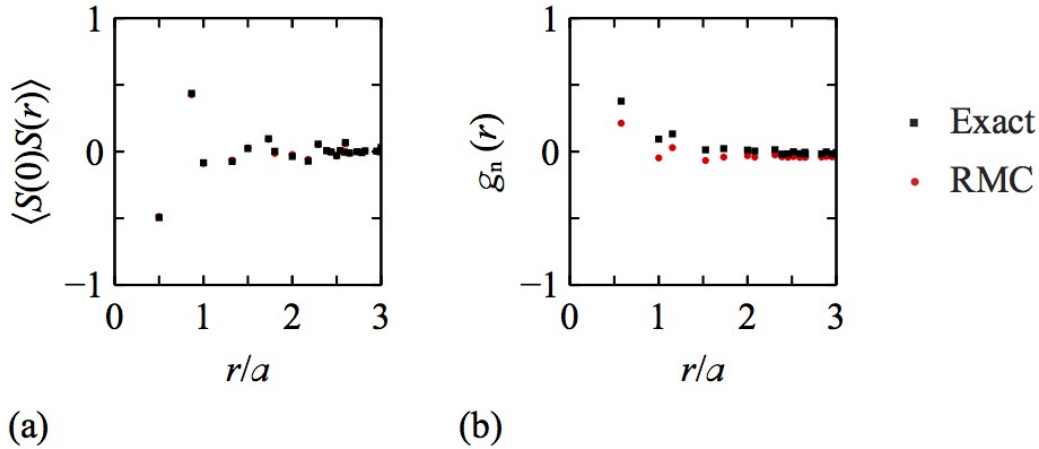


Figure 4. (a) Radial spin correlation function $\langle \mathbf{S}(0) \cdot \mathbf{S}(r) \rangle$. Exact values (from direct Monte Carlo simulations) are shown as black squares, and values obtained from the SPINVERT fit to powder data are shown as red circles. The SPINVERT values are near-identical to the exact values. (b) Nematic spin correlation function $g_n(r)$ defined in the text. Exact values are shown as black squares, and values obtained from the SPINVERT fit are shown as red circles. The SPINVERT fit correctly determines the trend in nematic correlations, but underestimates the magnitude by $\sim 50\%$.

is the vector normal to the plane formed by the three spins of a triangle. The comparison of the SPINVERT $g_n(r)$ with the exact result is shown in Fig. 4(b). It is apparent that SPINVERT consistently underestimates the value of $g_n(r)$ by around 50%. Thus it seems that SPINVERT is somewhat less sensitive to higher-order spin correlations than to spin-pair correlations. Conversely, since the experimental data are only directly sensitive to spin-pair correlations, it is perhaps surprising that RMC should show any sensitivity to higher-order correlations at all.

Finally, we consider the directional dependence of the real-space spin correlations. The correlation functions we have plotted so far are radial averages, which take no account of the geometry of the kagome lattice. However, this must obscure a great deal of information—after all, it is the geometry of the lattice which leads to frustration. In order to represent the directional dependence of the correlations, we consider the two-dimensional spin correlation function $\langle \mathbf{S}(\mathbf{0}) \cdot \mathbf{S}(\mathbf{r}) \rangle$. This function is seldom shown in the literature (although its Fourier transform $I(\mathbf{Q})$ is frequently given), but it can reveal surprisingly simple patterns in the paramagnetic structure [36]. For a Bravais lattice, $\langle \mathbf{S}(\mathbf{0}) \cdot \mathbf{S}(\mathbf{r}) \rangle$ is straightforward to calculate: one simply calculates the dot product of a central spin with the spin at displacement \mathbf{r} away, and averages over each spin as a centre. For a non-Bravais lattice, such as kagome, the calculation is slightly more involved, because different basis atoms can be related to each other by rotational as well as translational symmetries. In such cases, it is necessary to rotate our coordinate axes when moving between basis atoms such that each atom is in an equivalent environment. For the kagome lattice, with a three-atom basis, a set of suitable local axes are shown in Fig. 2. The directional dependence of the spin correlations is shown in Fig. (5). The “Exact” spin correlations for the starting model [Fig. (5), left panel] show a non-trivial dependence on both distance and angle, yet the

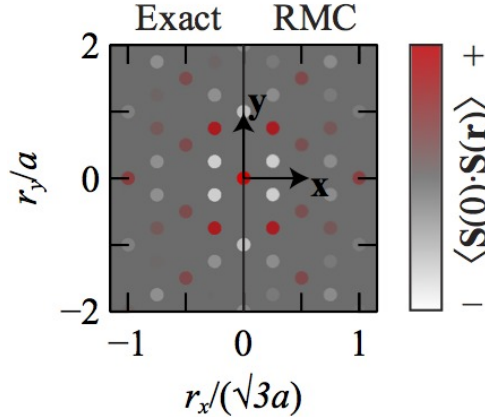


Figure 5. Two-dimensional spin correlation function $\langle \mathbf{S}(\mathbf{0}) \cdot \mathbf{S}(\mathbf{r}) \rangle$ for the Heisenberg kagome antiferromagnet. The left panel shows exact values, and the right panel shows values obtained from SPINVERT refinement of powder data. The x and y axes are the local axes given in Fig. 2.

result from SPINVERT refinement reproduces all the main features of this dependence [Fig. (5), left panel].

An obvious question which remains is: how well do these results transfer to actual experimental data? Compared with the simulated data used above, real data are likely to have a somewhat more limited Q -range, and to contain a certain amount of statistical noise. We will now consider the effects of these limitations, and make some suggestions as to the kind of data which are suitable for SPINVERT refinement.

We investigate the effect of limited Q -range on the predicted single-crystal scattering patterns by identifying two extreme scenarios. First, we attempt a refinement omitting all the data except the main diffuse peak, by setting $Q'_{\max} = 2.5$ [Fig. 6(a)]. Then we consider the inverse situation, omitting all the data below $Q'_{\min} = 2.5$ but keeping the subsequent peaks [Fig. 6(b)]. As anticipated, in both cases the reconstruction of the single-crystal scattering is of lower quality than for the full refinement. What is surprising is that both refinements nevertheless reproduce the main features of the diffuse scattering. Moreover, the overall quality of both reconstructions is similar, even though the input data do not overlap in Q . This behaviour can be understood by recognising that the diffuse scattering pattern is periodic in reciprocal space, and this periodicity is dictated by the crystal structure [17]. Consequently, the powder-averaged scattering from subsequent Brillouin zones contains information about the first Brillouin zone, and *vice versa*. In effect, every measured value of Q represents an average over a different selection of points in the first Brillouin zone, so that increasing Q_{\max} places increasingly stronger restrictions on $I(\mathbf{Q})$.

Does this mean it is best to measure data to the highest possible Q_{\max} ? In practice, the answer is probably only a qualified “yes”. An exception is that the behaviour of the single-crystal scattering in the limit $\mathbf{Q} \rightarrow \mathbf{0}$ is uniquely determined by the powder scattering as $Q \rightarrow 0$. This limit is generally less experimentally accessible for larger values of Q_{\max} . As a result, if there is insufficient information in the data as a whole to constrain the low- Q behaviour, there is a tendency for SPINVERT refinement

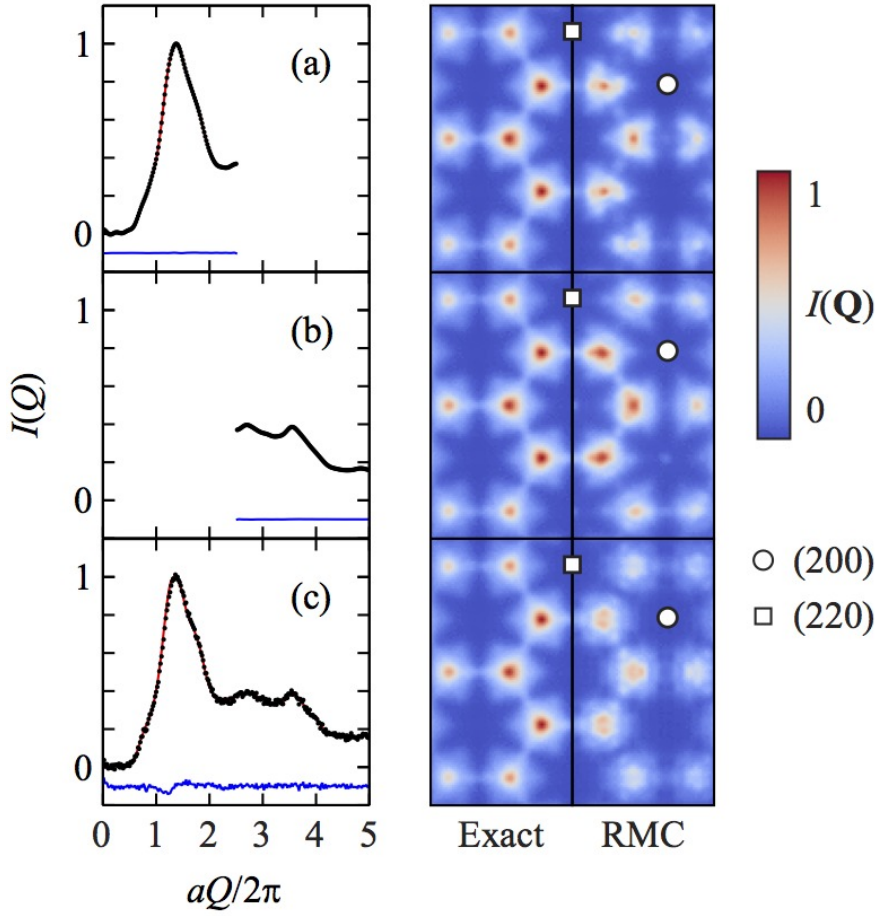


Figure 6. (a) Fit to powder data and predicted single-crystal scattering pattern for input powder data with limited $Q'_{\max} = 2.5$. Input data are shown as black circles, fit as a red line, and difference (data–fit) as a blue line. (b) Fit to powder data and predicted single-crystal scattering pattern for input powder data with $Q'_{\min} = 2.5$. (c) Fit to powder data and predicted single-crystal scattering pattern for input powder data containing statistical noise, as described in the text.

to refine inaccurate values for $I(Q \rightarrow 0)$. An example of this behaviour can be seen in Fig. 6b. Another consideration is that, as the scattering becomes weaker at higher Q , the experimental errors become proportionately larger, and fitting to errors in the high- Q data may produce noise even at low- Q in the predicted single-crystal patterns. We may therefore ask how low the statistical errors need to be. To test this, we added a small amount of statistical noise to our simulated data and repeated the SPINVERT refinement. The noise was simulated by choosing random numbers from a Gaussian distribution with standard deviation $\sigma = 0.01$ (corresponding to an error of 1% in the most intense data point). With these (relatively small) errors, we find that the single crystal pattern predicted by fitting the powder data is noticeably reduced in quality [Fig. 6(c)], although the main features are still recovered.

We therefore draw two main conclusions regarding the data quality which is

desirable for SPINVERT refinement. First, the differences between Fig. 3 and Fig. 6(c) suggest that *it is important to measure beyond just the first peak in the scattering pattern*. Second, it is essential that *the statistical errors in the data are low*; specifically, they should be low enough that the modulation in the powder scattering pattern is well resolved even at high values of Q . While these criteria may be difficult to achieve with samples that are small or very highly absorbing (particularly if the material in question also has a small S), in most other cases they should be attainable using current-generation diffuse-scattering diffractometers such as D7 (ILL) [37] or DNS (Jülich) [38]. Refinement of experimental data using SPINVERT is therefore likely to be both practical and informative—a point we hope to demonstrate in the following section.

6. Legacy data: $\text{Y}_{0.5}\text{Ca}_{0.5}\text{BaCo}_4\text{O}_7$

As our final case study we demonstrate one of the key uses we envisage for the SPINVERT program: analysis of legacy data. We consider spin correlations in the compound $\text{Y}_{0.5}\text{Ca}_{0.5}\text{BaCo}_4\text{O}_7$ [15]. Based on powder diffuse scattering data, this compound was originally suggested to realise a kagome-lattice model similar to that studied in Section 5 [15]. However, subsequent single-crystal experiments on the parent compound YBaCo_4O_7 suggested a different picture [39]. Here we attempt to reconcile these two sets of results, by using the original powder data of Ref. [15] to predict the single-crystal data obtained in Ref. [39].

The crystal structure of $\text{Y}_{0.5}\text{Ca}_{0.5}\text{BaCo}_4\text{O}_7$ (hexagonal $P6_3mc$ [40] or trigonal $P31c$ [41]) has a unit cell containing eight magnetic Co ions, spread over two inequivalent sites (Co1 and Co2). The Co1 sites form triangular layers and the Co2 sites kagome layers, with the two kinds of layers alternating along the c axis, identifying the potential for spin frustration [Fig. 7]. The Co1 atoms are in the Co^{3+} valence state, and the Co2 atoms are mixed-valence Co^{3+} and Co^{2+} ; both Co sites are tetrahedrally coordinated by oxygen. The spin correlations in $\text{Y}_{0.5}\text{Ca}_{0.5}\text{BaCo}_4\text{O}_7$ were first studied in detail in Ref. [15]. In that study, polarised-neutron powder diffraction data showed the absence of periodic magnetic order to $T = 1.2\text{ K}$. It was considered that this lack of magnetic order suggested that the kagome planes were essentially decoupled. This was explained by postulating that the Co1 (triangular lattice) ions are low-spin $S = 0$, rather than high-spin $S = 2$ as might be expected. The experimental basis for this model was that the magnetic moment obtained from fitting the neutron scattering data was significantly lower than the calculated value assuming that both Co sites were high-spin. However, several subsequent studies have suggested a need for this conclusion to be revised. First, an inelastic neutron scattering study [41] shows that a high-frequency component to the spin fluctuations is present, which lies beyond the dynamic range of the measurements performed in Ref. [15]. When this component to the scattering is taken into account, the expected moment for a model with both Co sites high-spin is recovered. Second, X-ray absorption spectra measurements for the parent compound, YBaCo_4O_7 , indicate that both Co sites are high-spin [42]. It was also noted that in T_d symmetry an $S = 0$ state for Co requires two spins to align parallel in a t_2 orbital, in disagreement with Hund’s first rule. To allow a $S = 0$ state a very large distortion from T_d symmetry would be required, whereas the crystal structure, as determined by neutron diffraction, shows only a small distortion to C_{3v} [41].

Perhaps most significant is a study reporting single-crystal neutron scattering

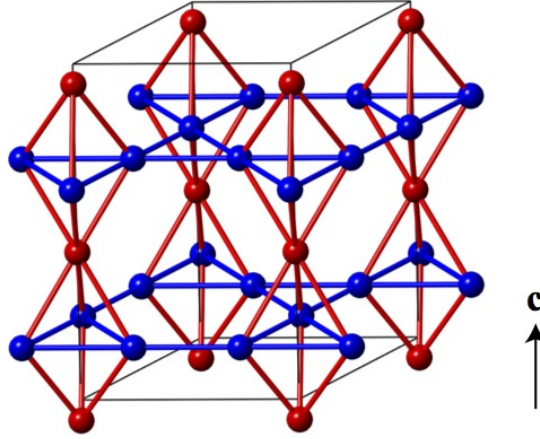


Figure 7. Arrangement of magnetic Co ions in $\text{Y}_{0.5}\text{Ca}_{0.5}\text{BaCo}_4\text{O}_7$. The Co2 ($\text{Co}^{2+}/\text{Co}^{3+}$) sites form kagome layers, shown in blue. The Co1 (Co^{3+}) sites form triangular layers, shown in red. The structure can be described as a network of corner-sharing trigonal bipyramids.

measurements of the parent compound, YBaCo_4O_7 [39]. Unlike $\text{Y}_{0.5}\text{Ca}_{0.5}\text{BaCo}_4\text{O}_7$, oxygen-stoichiometric YBaCo_4O_7 undergoes a transition to an antiferromagnetic state at $T_N \simeq 110$ K [43]. Just above T_N , at $T = 130$ K, broad diffuse features were observed in the $(hk0)$ reciprocal-space plane, indicating short-range magnetic order within the kagome planes. Most interestingly, much sharper magnetic peaks were also observed in the perpendicular scattering plane, identifying the presence of longer-range correlations along the c axis. These features were successfully reproduced using a spin Hamiltonian in which both Co sites are magnetic: it was found that Co1 spins align ferromagnetically with a long correlation length, whereas the Co2 kagome spins remain in a spin-liquid-like state.

An outstanding question is then: do the spin correlations in $\text{Y}_{0.5}\text{Ca}_{0.5}\text{BaCo}_4\text{O}_7$ resemble the model of independent kagome planes of Co2 spins proposed in Ref. [15], or do they follow the model of ferromagnetic correlations between Co1 spins identified in Ref. [39] for YBaCo_4O_7 ? The lack of single-crystal samples of $\text{Y}_{0.5}\text{Ca}_{0.5}\text{BaCo}_4\text{O}_7$ renders a direct answer inaccessible. However, we will show that a reasonably conclusive answer can nevertheless be obtained by employing SPINVERT refinement of the original powder data of Ref. [15]. We note the existence of a previous RMC study $\text{Y}_{0.5}\text{Ca}_{0.5}\text{BaCo}_4\text{O}_7$ using different data and refinement software [41]; our results are in broad agreement with this study, but go beyond it by addressing the three-dimensional nature of the spin correlations. We performed SPINVERT refinements using a $10 \times 6 \times 6$ supercell of the orthorhombic unit cell containing 5760 spins (crystallographic details are taken from Ref. [40]). In our refinements, we assume both Co sites are magnetic. As a starting point, we also take the magnetic moments on both Co sites to be of equal magnitude; refinements were also performed assuming relative spin lengths $S = 2$ (for Co^{3+}) and $S = 3/2$ (for Co^{2+}), which gave similar results. Refinements were performed for 300 proposed moves per spin, after which time

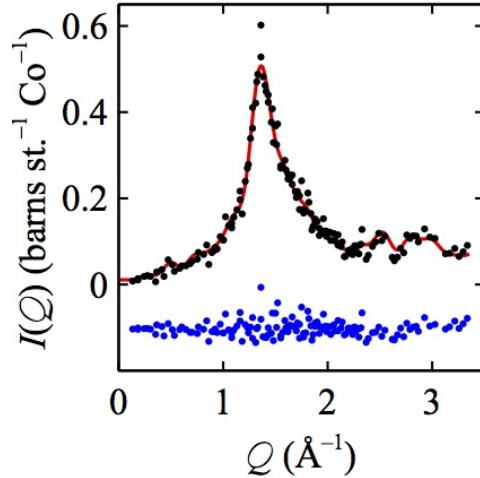


Figure 8. Powder magnetic diffuse scattering data for $\text{Y}_{0.5}\text{Ca}_{0.5}\text{BaCo}_4\text{O}_7$ from Schweika et al. The temperature of data collection for the powder data $T = 1.2$ K. Experimental data are shown as black circles, SPINVERT fit as a red line, and difference (data-fit) as blue circles.

no significant improvement was observed in χ^2 , and 16 independent refinements were performed in order to obtain good statistics for scattering calculations. An intensity scale factor was allowed to refine to fit the data, from which we estimate $S \simeq 1.1$ (taking $g = 2$), in good agreement with the results of [41, 15]. The fit-to-data we obtain is shown in Fig. 8. All the features of the data are captured very well, apart from a slight peak broadening in the fit due to the finite box size.

Having obtained spin configurations in agreement with the experimental data, we proceed to characterise the nature of the spin correlations. First we use the SPINDIFF program to calculate the single-crystal scattering pattern from the SPINVERT spin configurations. This allows a direct comparison between our prediction of the single-crystal scattering for $\text{Y}_{0.5}\text{Ca}_{0.5}\text{BaCo}_4\text{O}_7$ and the experimental single-crystal data for YBaCo_4O_7 from Ref. [39]. This comparison is shown in Fig. 9. Strikingly, the experimental data and the SPINVERT prediction are almost identical. Particularly significant is that the sharp reflections at $(\frac{1}{2}02)$ are present in both the SPINVERT refinement and the single-crystal data. We note that the SPINVERT refinements are performed starting from entirely random spin configurations, so these sharp features cannot appear by chance: they must be required by the input powder data. Therefore, a model of decoupled kagome planes with conventional antiferromagnetic correlations (as considered in Section 5) is ruled out. Indeed, there are qualitative differences between the powder diffuse scattering for such a model [Fig. 3] and the experimental powder data shown in Fig. 8.

Following Ref. [39] we plot the spin correlations along two directions in real space. In Fig. 10, we show correlations along hexagonal [100]-type directions within the kagome plane (blue circles), and along the [001] directions (red squares). The correlations along [100] are antiferromagnetic and relatively weak. The correlations along [001] are always ferromagnetic, and are significantly stronger, with exponential correlation length $\xi \approx 13$ Å. In these essential features, the correlation functions we

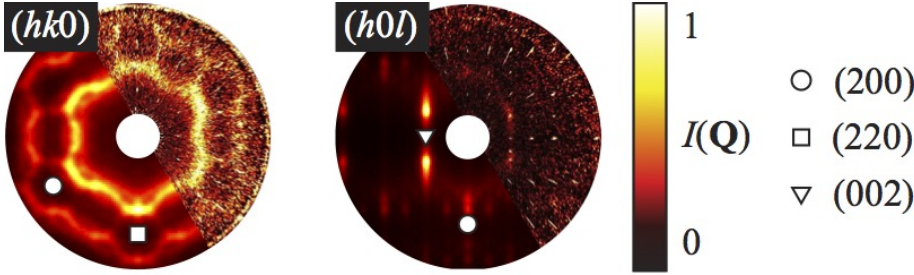


Figure 9. Comparison of predicted magnetic diffuse scattering for $\text{Y}_{0.5}\text{Ca}_{0.5}\text{BaCo}_4\text{O}_7$ with experimental data for YBaCo_4O_7 . Two reciprocal-space planes are shown, $(hk0)$ [left-hand image] and $(h0l)$ [right-hand image]. For each plane, the left panel shows the predicted single-crystal scattering based on fitting the $T = 1.2\text{ K}$ powder data of Schweika *et al.* for $\text{Y}_{0.5}\text{Ca}_{0.5}\text{BaCo}_4\text{O}_7$ [15], and the right panel shows the experimental single-crystal data of Manuel *et al.* for YBaCo_4O_7 at $T = 130\text{ K}$ [39].

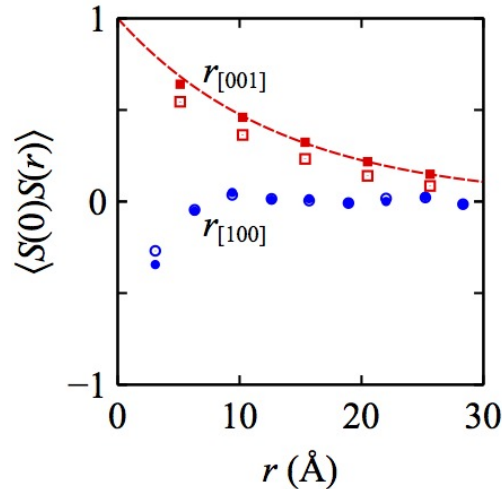


Figure 10. Spin correlation function for $\text{Y}_{0.5}\text{Ca}_{0.5}\text{BaCo}_4\text{O}_7$ calculated from SPINVERT. Red squares show ferromagnetic correlations along the $[001]$ real-space direction (c -axis). Blue circles show antiferromagnetic correlations along (100) -type directions within the kagome planes. Filled points are values obtained from refinements assuming magnetic moments of equal length for both Co sites; hollow points assume $S = 2$ for Co^{3+} and $S = 3/2$ for Co^{2+} .

have shown agree closely with the model for YBaCo_4O_7 (Fig. 3 of Ref. [39]). We note that a quantitative comparison is not possible with the correlation functions shown in Ref. [39]: their results were obtained from direct Monte Carlo simulations at an arbitrary low temperature, and hence will show much stronger short-range order than we observe for $\text{Y}_{0.5}\text{Ca}_{0.5}\text{BaCo}_4\text{O}_7$. However, all the qualitative features, both in real and reciprocal space, are in excellent agreement.

In conclusion, we have found that the spin correlations in $\text{Y}_{0.5}\text{Ca}_{0.5}\text{BaCo}_4\text{O}_7$ closely resemble those in YBaCo_4O_7 . The degree of resemblance is remarkable, given that there is a difference in the temperature of data collection of two orders

of magnitude between the single-crystal data of Ref. [39] and the powder data of Ref. [15]. This result may be explained by the substitution of Ca for Y in $Y_{0.5}Ca_{0.5}BaCo_4O_7$, which introduces disorder into the exchange pathways, in effect reducing the strength of the magnetic interactions. This disorder may also help explain why $Y_{0.5}Ca_{0.5}BaCo_4O_7$ fails to order magnetically, although the mechanism by which order is prevented is not yet understood. Perhaps most importantly, the observation that the key features of single-crystal data can be reproduced by fitting *powder* data for a real system presents several opportunities. In the family of compounds based on $YBaCo_4O_7$, it was recently suggested that chiral order may be present in the paramagnetic phase [44]: the appropriate correlation functions are readily calculable using RMC techniques, so this intriguing possibility could be in principle be investigated using SPINVERT. More generally, we would argue that the initial uncertainty about the nature of the spin correlations in $Y_{0.5}Ca_{0.5}BaCo_4O_7$ may have arisen partially from a desire to impose a model onto experimental data, rather than *vice versa*. The essential advantage of the reverse Monte Carlo approach is that the refinement is entirely data-driven, so there is no requirement to think in terms of paradigms of frustrated magnetism (*e.g.*, independent kagome sheets) when performing initial data analysis. Reality may be more complex than the models we imagine; the RMC approach recognises this, and presents us with results which are essentially model-independent.

Conclusions

In this paper we have detailed the SPINVERT program for refinement of paramagnetic powder scattering data using a reverse Monte Carlo approach. This method is capable of reconstructing the three-dimensional magnetic neutron scattering pattern from spherically-averaged data [13]. In addition, all the spin correlation functions of the system are accessed. The RMC technique is primarily sensitive to spin-pair correlations; however, in favourable cases we recover information about higher-order spin correlations. We have not considered here whether information on single-ion anisotropy can be obtained, preferring to treat the anisotropy as a structural constraint. However, we anticipate that the technique may also have a limited degree of sensitivity to single-ion effects in systems with relatively low crystal symmetry.

A key point about RMC is that it is entirely independent of a spin Hamiltonian. This may be an advantage or a disadvantage: an advantage, because it is not necessary to assume a form of the Hamiltonian to model the spin correlations; a disadvantage, because it does not produce such a microscopic model as output. Compared to other model-independent techniques for analysis of diffuse scattering (such as simple curve fitting), we believe that the RMC approach is superior in both the quantity and accuracy of information it provides. Most importantly, the crystal structure is a key ingredient in RMC refinements. Knowledge of the crystal structure places strong constraints on the form of the magnetic correlations, and it is this extra information allows the three-dimensional scattering function $I(\mathbf{Q})$ and spin correlation function $\langle \mathbf{S}(\mathbf{0}) \cdot \mathbf{S}(\mathbf{r}) \rangle$ to be reconstructed. In fact, the key point here may not relate directly to RMC at all: it is simply that the magnetic powder diffraction data—together with knowledge of the the crystal structure—contain a great deal of information. It seems very likely that other techniques could be developed to access this information effectively; for example, it is possible to fit interaction parameters directly to powder data within a mean-field theory model (see, *e.g.*, [45, 46]).

There are also certain disadvantages to the RMC approach. Most importantly, RMC tends to produce the most disordered spin configuration compatible with experimental data [12]. In practice, we have not found the extent to which disorder is overestimated to be too great, provided the spin anisotropy is specified for Ising or XY systems [13]. However, it is not possible to know in advance the extent to which disorder will be created for a given dataset. It is important always to remember that the success of RMC depends entirely on the quality of the data with which it is provided. The data should show the whole of the first broad peak as well as some of the subsidiary peaks, and should ideally have excellent statistics. The lowest possible background is desirable, and for this reason polarised-neutron diffraction data have significant advantages [37]. We also anticipate that RMC may be less successful for crystal structures which are complex—in the sense that they contain many radial separations between pairs of atoms which nearly overlap—since the effect of the limited real-space resolution imposed by Q_{\max} will then become more significant.

We hope that the SPINVERT program will be useful in several situations. One possible use is the re-analysis of legacy data, as exemplified in Section 6. More importantly, when large single crystal samples are currently unavailable, single crystal-like information can be obtained using SPINVERT by fitting high-quality powder data. A few topical examples should illustrate the potential for discovery. For example, the $S = 1/2$ kagome system kapellasite was recently synthesised [47], with measurements of the bulk properties and inelastic neutron scattering suggesting a quantum spin-liquid phase [48]. In the absence of single-crystal samples, SPINVERT refinement of powder data would allow detailed characterisation of these spin-liquid correlations. Second, “the metallic spin ice” system $\text{Pr}_2\text{Ir}_2\text{O}_7$ [49] exhibits a range of seemingly unique properties, including a spontaneous Hall effect in the paramagnetic phase suggestive of chiral order [4]. Only small single crystals ($\sim 1\text{ mm}^3$) are reported [50], so SPINVERT refinement of powder diffraction data would allow a valuable comparison of the predicted $I(\mathbf{Q})$ with microscopic models [51]. Furthermore, the ability of SPINVERT to use a structural model containing non-magnetic impurities would allow studies of canonical frustrated spin glasses such as $\text{SrCr}_{9x}\text{Ga}_{12-9x}\text{O}_{19}$ (SCGO) (see, *e.g.*, [52, 53]) and $\text{Ba}_2\text{Sn}_2\text{ZnGa}_{10-7x}\text{Cr}_{7x}\text{O}_{22}$ (BSZCGO) [54]: a model of the structural disorder could be produced using, *e.g.*, pair distribution function techniques [55], and this structural model used as a starting-point for SPINVERT refinement of magnetic diffraction data. In this way, the impact of the structural disorder on the magnetic correlations could be compared with theoretical models [56]. Finally, in some cases it may even be advantageous to perform experiments on powder samples: for example, for high-throughput studies, for highly-absorbing samples [57], or when only small single crystals are available. Consequently, we believe that the SPINVERT code—available at <http://spinvert.chem.ox.ac.uk>—will enable useful information to be obtained for a much wider range of cooperative paramagnets than is presently the case.

Acknowledgments

We are grateful to M. J. Cliffe, M. J. Gutmann, P. Manuel, L. C. Chapon, D. A. Keen, and B. D. Rainford for valuable discussions. JAMP and ALG gratefully acknowledge financial support from the STFC, EPSRC (EP/G004528/2) and ERC (Ref: 279705).

References

- [1] Castelnovo C, Moessner R and Sondhi S L 2008 *Nature* **451** 42–45
- [2] Fennell T, Deen P P, Wildes A R, Schmalzl K, Prabhakaran D, Boothroyd A T, Aldus R J, McMorrow D F and Bramwell S T 2009 *Science* **326** 415–417
- [3] Han T H, Helton J S, Chu S, Nocera D G, Rodriguez-Rivera J A, Broholm C and Lee Y S 2012 *Nature* **492** 406–410
- [4] Machida Y, Nakatsuji S, Onoda S, Tayama T and Sakakibara T 2010 *Nature* **463** 210–213
- [5] Villain J 1979 *Phys. B.* **33** 31
- [6] Isakov S V, Gregor K, Moessner R and Sondhi S L 2004 *Phys. Rev. Lett.* **93** 167204
- [7] Wills A 2001 *J. Phys. IV France* **11** 133–158
- [8] McGreevy R L and Puzsai L 1988 *Mol. Simul.* **1** 359–367
- [9] Keen D A, Bewley R I, Cywinski R and McGreevy R L 1996 *Phys. Rev. B* **54**(2) 1036–1042
- [10] Goodwin A L, Tucker M G, Dove M T and Keen D A 2006 *Phys. Rev. Lett.* **96** 047209
- [11] Laver M, Forgan E M, Abrahamsen A B, Bowell C, Geue T and Cubitt R 2008 *Phys. Rev. Lett.* **100**(10) 107001
- [12] McGreevy R L 2001 *J. Phys.: Condens. Matter* **13** R877
- [13] Paddison J A M and Goodwin A L 2012 *Phys. Rev. Lett.* **108**(1) 017204
- [14] Park J, Park J G, Jeon G S, Choi H Y, Lee C, Jo W, Bewley R, McEwen K A and Perring T G 2003 *Phys. Rev. B* **68**(10) 104426
- [15] Schweika W, Valldor M and Lemmens P 2007 *Phys. Rev. Lett.* **98**(6) 067201
- [16] Granado E, Lynn J W, Jardim R F and Torikachvili M S 2013 *Phys. Rev. Lett.* **110**(1) 017202
- [17] Enjalran M and Gingras M J P 2004 *Phys. Rev. B* **70**(17) 174426
- [18] Chalker J T, Holdsworth P C W and Shender E F 1992 *Phys. Rev. Lett.* **68** 855–858
- [19] Reimers J N and Berlinsky A J 1993 *Phys. Rev. B* **48**(13) 9539–9554
- [20] Tucker M G, Keen D A, Dove M T, Goodwin A L and Hui Q 2007 *J. Phys.: Condens. Matter* **19** 335218
- [21] Blech I A and Averbach B L 1964 *Physics* **1** 31–44
- [22] Metropolis N and Ulam S 1949 *J. Am. Stat. Assoc.* **44** 335–341
- [23] Proffen T and Welberry T R 1997 *Acta Crystallogr. A* **53** 202–216
- [24] Squires G L 1978 *Introduction to the theory of thermal neutron scattering* (Cambridge University Press)
- [25] Bertaut E and Burlet P 1967 *Solid State Commun.* **5** 279 – 283 ISSN 0038-1098
- [26] Schärpf O and Capellmann H 1993 *Phys. Stat. Solidi A* **135** 359–379 ISSN 1521-396X
- [27] Rotter M and Boothroyd A T 2009 *Phys. Rev. B* **79**(14) 140405
- [28] Cliffe M J, Dove M T, Drabold D A and Goodwin A L 2010 *Phys. Rev. Lett.* **104** 125501
- [29] Billinge S J L 2010 *Physics* **3** 25
- [30] Bramwell S T 2011 *Introduction to Frustrated Magnetism* (Springer) chap Neutron Scattering and Highly Frustrated Magnetism
- [31] Butler B D and Welberry T R 1992 *J. Appl. Crystallogr.* **25** 391–399
- [32] Chubukov A 1992 *Phys. Rev. Lett.* **69**(5) 832–835
- [33] Wills A and Harrison A 1996 *J. Chem. Soc., Faraday Trans.* **92** 2161–2166
- [34] Fåk B, Coomer F C, Harrison A, Visser D and Zhitomirsky M E 2008 *Europhys. Lett.* **81** 17006
- [35] de Vries M A, Stewart J R, Deen P P, Piatek J O, Nilsen G J, Rønnow H M and Harrison A 2009 *Phys. Rev. Lett.* **103**(23) 237201
- [36] Paddison J A M, Stewart J R, Manuel P, Courtois P, McIntyre G J, Rainford B D and Goodwin A L 2013 *arXiv:1302.0833*
- [37] Stewart J R, Deen P P, Andersen K H, Schober H, Barthélémy J F, Hillier J M, Murani A P, Hayes T and Lindenau B 2009 *J. Appl. Crystallogr.* **42** 69–84
- [38] Schweika W and Böni P 2001 *Physica B: Condens. Matter* **297** 155 – 159 ISSN 0921-4526
- [39] Manuel P, Chapon L C, Radaelli P G, Zheng H and Mitchell J F 2009 *Phys. Rev. Lett.* **103** 037202
- [40] Valldor M 2006 *Solid State Sci.* **8** 1272 – 1280 ISSN 1293-2558
- [41] Stewart J R, Ehlers G, Mutka H, Fouquet P, Payen C and Lortz R 2011 *Phys. Rev. B* **83**(2) 024405
- [42] Hollmann N, Hu Z, Valldor M, Maignan A, Tanaka A, Hsieh H H, Lin H J, Chen C T and Tjeng L H 2009 *Phys. Rev. B* **80**(8) 085111
- [43] Chapon L C, Radaelli P G, Zheng H and Mitchell J F 2006 *Phys. Rev. B* **74**(17) 172401
- [44] Khalyavin D D, Manuel P and Chapon L C 2012 *Phys. Rev. B* **85**(22) 220401
- [45] Yavors’kii T, Enjalran M and Gingras M J P 2006 *Phys. Rev. Lett.* **97**(26) 267203
- [46] Skoulatos M, Goff J P, Geibel C, Kaul E E, Nath R, Shannon N, Schmidt B, Murani A P, Deen

- P P, Enderle M and Wildes A R 2009 *Europhys. Lett.* **88** 57005
- [47] Colman R H, Ritter C and Wills A S 2008 *Chem. Mater.* **20** 6897–6899
- [48] Fåk B, Kermarrec E, Messio L, Bernu B, Lhuillier C, Bert F, Mendels P, Koteswararao B, Bouquet F, Ollivier J, Hillier A D, Amato A, Colman R H and Wills A S 2012 *Phys. Rev. Lett.* **109**(3) 037208
- [49] Nakatsuji S, Machida Y, Maeno Y, Tayama T, Sakakibara T, Duijn J v, Balicas L, Millican J N, Macaluso R T and Chan J Y 2006 *Phys. Rev. Lett.* **96**(8) 087204
- [50] Machida Y, Nakatsuji S, Maeno Y, Tayama T and Sakakibara T 2007 *J. Magn. Magn. Mater.* **310** 1328 – 1330
- [51] Ikeda A and Kawamura H 2008 *J. Phys. Soc. Jpn.* **77** 073707
- [52] Broholm C, Aeppli G, Espinosa G P and Cooper A S 1990 *Phys. Rev. Lett.* **65**(25) 3173–3176
- [53] Iida K, Lee S H and Cheong S W 2012 *Phys. Rev. Lett.* **108**(21) 217207
- [54] Hagemann I S, Huang Q, Gao X P A, Ramirez A P and Cava R J 2001 *Phys. Rev. Lett.* **86**(5) 894–897
- [55] Young C A and Goodwin A L 2011 *J. Mater. Chem.* **21**(18) 6464–6476
- [56] Sen A, Damle K and Moessner R 2011 *Phys. Rev. Lett.* **106**(12) 127203
- [57] Stewart J R, Ehlers G, Wills A S, Bramwell S T and Gardner J S 2004 *J. Phys.: Condens. Matter* **16** L321